Design of a Compliant Gripper with Multi-mode Jaws

Guangbo Hao[1,*], Haiyang Li[1], Abhilash Nayak[2], Stephane Caro[3]

[1]School of Engineering-Electrical and Electronic Engineering, University College Cork, Cork, Ireland
[2]Ecole Centrale de Nantes, Laboratoire des Sciences du Numérique de Nantes (LS2N), Nantes, France
[3]CNRS, Laboratoire des Sciences du Numérique de Nantes (LS2N), Nantes, France
Corresponding author: G.Hao@ucc.ie

Abstract: This paper presents the design of a multi-mode compliant gripper, using the singularities of the four-bar mechanism with equilateral links. The mobility of the compliant gripper can be reconfigurable to grasp a variety of shapes or adapt to specific requirements. The compliant gripper is a compact and two-layer structure. Two linear actuators are required to enable the multiple operation modes, by the conversion of two pairs of slider-crank mechanisms. A multi-mode compliant four-bar mechanism is first presented and kinematically analysed. The design and the kinetostatic modelling of the resulting compliant gripper are then performed. Finally, the analysis of the reconfigurable compliant gripper under different actuation schemes is carried out, including the comparison of the results obtained from analytical modelling, finite element analysis and experimental testing.

1. Introduction

A recent and significant part of the paradigm shift brought forth by the industrial revolution is the miniaturization of electromechanical devices. Along with the reduction of size, miniaturization reduces the cost, energy and material consumption. On the other hand, the fabrication, manipulation and assembly of miniaturized components is difficult and challenging. Grippers are grasping tools for various objects, which have been extensively used in different fields such as material handling, manufacturing and medical devices [1]. Traditional grippers are usually composed of rigid-body kinematic joints, which have issues associated with friction, wear and clearance/backlash [2]. Those issues lead to poor resolution and repeatability of grasping motion, which makes the high-precision manipulation of miniaturized components challenging. In addition to being extremely difficult to grip sub-micrometre objects such as optical fibres and micro lens, traditional grippers are also very hard to grip brittle objects such as powder granular. This is because the minimal incremental motion (i.e. resolution) of the jaw in the traditional gripper is usually larger than the radius of the micro-object or already causes the breaking of the brittle object. Figure 1 shows a parallel-jaw gripper as an example. Although advanced control can be used to improve the gripper's resolution, its effort is trivial compared to the resulting high complexity and increased cost [2].

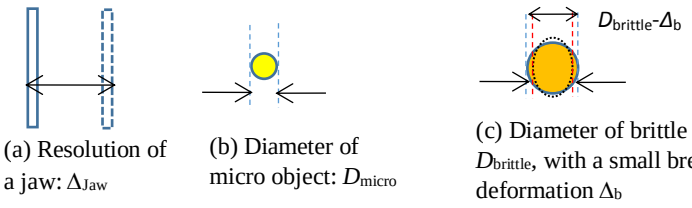

(a) Resolution of a jaw: Δ_{Jaw}

(b) Diameter of micro object: D_{micro}

(c) Diameter of brittle object: $D_{brittle}$, with a small breaking deformation Δ_b

$\Delta_{Jaw} > D_{micro}/2$
$\Delta_{Jaw} > \Delta_b/2$ (but $D_{brittle}$ can be larger than $2\Delta_{Jaw}$)

Figure 1: Comparison of traditional parallel-jaw gripper's resolution and size/deformation of objects

Although mechanisms are often composed of rigid bodies connected by joints, compliant mechanisms that include flexible elements as kinematic joints can be utilised to transmit a load and/or motion. The advances in compliant mechanisms have provided a new direction to address the above rigid-body problems easily [3]. The direct result of eliminating rigid-body kinematic joints removes friction, wear and backlash, enabling very high precision motions. In addition, it can be free of assembly when using compliant mechanisms so that miniaturization and monolithic fabrication are easily obtained.

There are mainly two approaches to design compliant grippers. The first one is the optimisation method [4] and the second is the kinematic substitution method [5]. The former optimizes the materials' distribution to meet specified motion requirements, which includes topology optimization, geometry optimization and size optimization. However, the optimization result often leads to sensitive manufacturing, and therefore minor fabrication error can largely change the output motion [6]. Also, the kinematics of the resulting gripper by optimization is not intuitive to engineers. The latter design method is very interesting since it takes advantage of the large number of existing rigid-body mechanisms and their existing knowledge. It renders a very clear kinematic meaning, which is easily used for shortening the design process. Parallel or closed-loop rigid-body architectures gain an upper hand here as their intrinsic properties favour the characteristics of compliant mechanisms like compactness, symmetry to reduce parasitic motions, low stiffness along the desired degrees of freedom (DOF) and high stiffness in other directions.

Moreover, compliant mechanisms usually work around a given (mostly singular) position for small range of motions (instantaneous motions). Therefore, parallel singular configurations existing in parallel manipulators may be advantageously exploited [7-12]. Parallel singularity can be an actuation singularity, constraint singularity or a compound singularity as explained in [7-9]. Rubbert et al used an actuation singularity to type-synthesize a compliant medical device [10, 11]. Another interesting kind of parallel singularity for a parallel manipulator that does not depend on the choice of actuation is a constraint singularity [12]. Constraint singularities may divide the workspace of a parallel manipulator into different operation modes resulting in a reconfigurable mechanism. Algebraic geometry tools have proved to be efficient in performing global analysis of parallel manipulators and recognizing their operation modes leading to mobility-reconfiguration [13-15]. The resulting mobility-reconfiguration can enable different modes of grasping in grippers. Thus, the reconfigurable compliant gripper unveils an ability to grasp a plethora of shapes or adapt to specific requirements unlike other compliant grippers in literature that exhibit only one (mostly parallel mode) of these grasping modes [16, 17].

Though there are abundant reconfigurable rigid-body mechanisms in the literature, the study of reconfigurable compliant mechanisms is limited. Hao studied the mobility and structure reconfiguration of compliant mechanisms [18] while Hao and Li introduced a position-space based structure reconfiguration approach to the reconfiguration of compliant mechanisms and to minimize parasitic motions [19]. Note that in rigid-body mechanisms, using the underactuated/adaptive grasping method [20,21], a versatile gripper for adapting to different shapes can be achieved. In this paper, one of the simplest yet ubiquitous parallel mechanisms, a four-bar linkage is considered at a constraint singularity configuration to design a reconfigurable compliant four-bar mechanism and then to construct a reconfigurable compliant gripper. From our best understanding, this is the first piece of work that considers a constraint singularity to design a reconfigurable compliant mechanism with multiple operation modes, also called motion modes.

This remaining of this paper is organised as follows. Section 2 describes the design of a multi-mode compliant four-bar mechanism and conducts the associated kinematic analysis. The multi-mode compliant gripper is proposed in Section 3 based on the work presented in Section 2, followed by the analytical kinetostatic modelling. A case study is discussed in Section 4, which shows the analysis of the gripper under different actuation schemes. Section 5 draws the conclusions.

2. Design of a multi-mode compliant four-bar mechanism

2.1 Compliant four-bar mechanism at its singularity position

A comprehensive singularity and operation mode analysis of a parallelogram mechanism is reported in [22], using algebraic geometry tools. As a specific case of the parallelogram mechanism, a four-bar linkage with equilateral links as shown in Fig. 2 is used in this paper, where the link length is l. Link AD is fixed, AB and CD are the cranks and BC is the coupler. Origin of the fixed frame, O_0 coincides with the centre of link AD while that of the moving frame O_1 with the centre of BC. The bar/link BC is designated as the output link with AB/CD as the input link. The location and orientation of the coupler with respect to the fixed frame can be denoted by (a, b, ϕ), where a and b are the Cartesian coordinates of point O_1 attached to the coupler, and ϕ is the orientation of the latter about z_0-axis, i.e., angle between x_0 and x_1 axes.

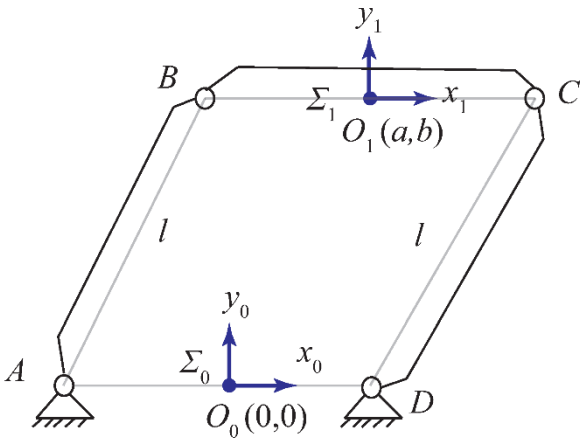

Figure 2: A planar equilateral four-bar linkage

The two constraint singularity positions of the equilateral four-bar linkage are identified in Fig. 3 [22]. At a constraint singularity, the mechanism may switch from one operation mode to another. Therefore, in case of the four-bar linkage with equal link lengths, the DOF at a constraint singularity is equal to 2. In this configuration, points A, B, C and D are collinear and the corresponding motion type is a translational motion along the normal to the line ABCD passing through the four points A, B, C and D, combined with a rotation about an axis directed along z_0 and passing through the line ABCD. Eventually, it is noteworthy that two actuators are required in order to control the end-effector in those constraint singularities in order to manage the operation mode changing.

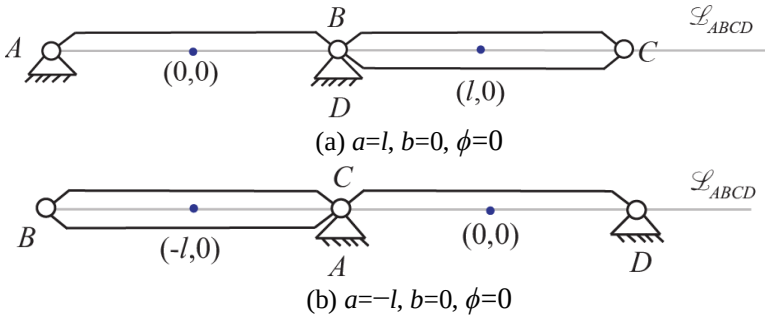

Figure 3: Constraint singular configuration of the planar equilateral four-bar linkage

Based on the constraint singularity configuration of the four-bar rigid-body mechanism represented in Fig. 3, a compliant four-bar mechanism can be designed through kinematically replacing the rigid rotational joints with compliant rotational joints [3, 5] in the singularity position. Note that, the singularity position (Fig. 3(a)) is the undeformed (home) configuration of the compliant mechanism. Each of the compliant rotational joints can be any type compliant rotational joint such as cross-spring rotational joint, notch rotational joint and cartwheel rotational joint [3].

In this section, the cross-spring rotational joint as the rotational/revolute joint (RJ) is employed to synthesize the design of a reconfigurable compliant four-bar mechanism based on the identified singularity (Fig. 4). In Fig. 4, the RJ-0 and RJ-2 are traditional cross-spring rotational joints, while both the RJ-1 and the RJ-3 are double cross-spring joints. Each of the two joints, RJ-1 and RJ-3, consists of two traditional cross-spring rotational joints in series with a common rotational axis and a secondary stage (encircled in Fig. 4). This serial arrangement creates symmetry and allows for greater motion and less stress in the mechanism. It should be mentioned that using these joints can allow large-amplitude motions compared to notch joints, which thus serves for illustrating the present concept easily. Note that these joints are not as compact and simple (with manufacture and precise issues) as circular notch joints. In addition, the parasitic rotational shift of these joints will be minimized if the beams intersect at an appropriate position of their length [23].

We specify that the Bar-0 is fixed to the ground and the Bar-2 is the output motion stage, also named coupler. Bar-1, Bar-2 and Bar-3 correspond to links, CD, BC, and AB, respectively, in Figure 3. The link length can be expressed as

$$l=L_B+L_R \quad (1)$$

where L_B and L_R are the lengths of each bar block and each compliant rotational joint, respectively, as indicated in Fig. 4.

Like the rigid-body four-bar mechanism shown in Fig. 3(a), the output motion stage (Bar-2) of the compliant four-bar mechanism has multiple operation modes under two rotational actuations (controlled by two input angles α and β for Bar-1 and Bar-3, respectively), as shown in Fig. 4. However, the compliant four-bar mechanism has more operation modes than its rigid counterpart as discussed below. A moving coordinate system (o-*xyz*) is defined in Fig. 4, which is located on Bar-2 (link BC), which coincides with the fixed frame (O-XYZ) in the singularity position. Based on this assumption, Bar-2's operation modes of the compliant four-bar mechanism are listed below:

a) Operation mode I: Rotation in the XY-plane about the Axis-L, when $\alpha \neq 0$ and $\beta = 0$.
b) Operation mode II: Rotation in the XY-plane about the Axis-R when $\alpha = 0$ and $\beta \neq 0$. In this mode, the cross-spring joints can tolerate this constrained configuration (close enough to the singularity) due to the induced small elastic extension of joints, but do not work as ideal revolute joints anymore.
c) Operation mode III: General rotation in the XY-plane about other axes except the Axis-L and Axis-R, when $\alpha \neq \beta$. Similar to the constraint in operation mode II, the cross-spring joints in this mode are no longer working as ideal revolute joints.
d) Operation mode IV: Pure translational motions in the XY-plane along the X- and Y-axes (mainly along the Y-axis), when $\alpha = \beta$.

It is noted that the rotational axes associated with α and β are both fixed axes (as indicated by solid lines in Fig. 4); while Axis-L and Axis-R (as indicated by dashed lines in Fig. 4) are both mobile axes. The rotational axis of α is the rotational axis of joint RJ-0, and the rotational axis of β is the rotational axis of joint RJ-3. Axis-L is the rotational axis of joint RJ-2, which moves as Bar-3 rotates. Axis-R is the rotational axis of joint RJ-1, which moves as Bar-1 rotates. As shown in Fig. 3, in the initial singular configuration, Axis-L overlaps with the axis of α; and Axis-R lies in the plane spanned by Axis-L and the Axis of β.

It should be also pointed out that it is possible for operation modes II and III having large-range motion thanks to the particular use of rotational joints which may not be true for circular notch joints anymore.

These operation modes are also highlighted in Fig. 5 with verification through the printed prototype. In order to simplify the analysis, let α and β be non-negative in Fig. 5. The primary motions of output motion stage (Bar-2) are the rotation in the XY plane and the translations along the X-and Y-axes; while the rotations in the XZ and YZ planes and translational motion along the Z-axis are the parasitic motions that are not the interest of this paper.

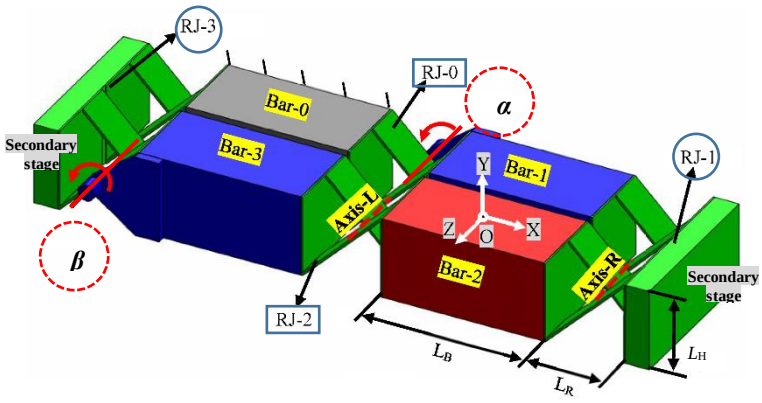

Figure 4: A compliant four-bar mechanism at its constraint singular position (as fabricated)

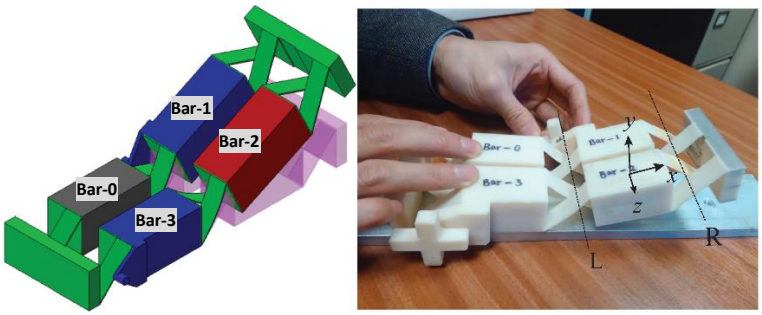

(a) Operation mode I: Rotation in the XY-plane about the Axis-L

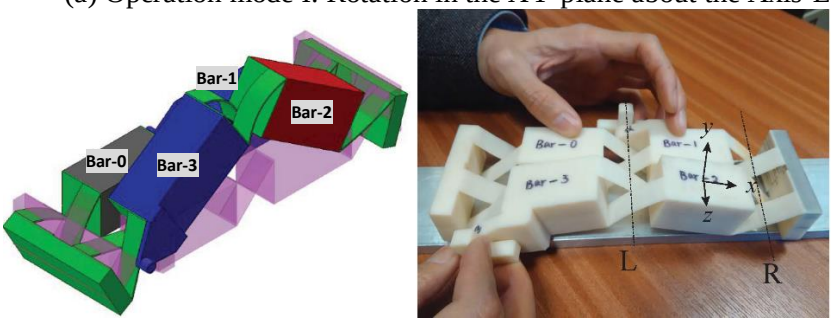

(b) Operation mode II: Rotation in the XY-plane about the Axis-R

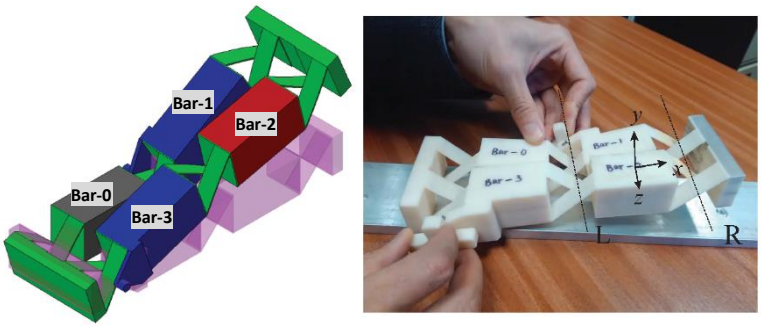

(c) Operation mode III: Rotation in the XY-plane about other axes except the Axis-L and Axis-R

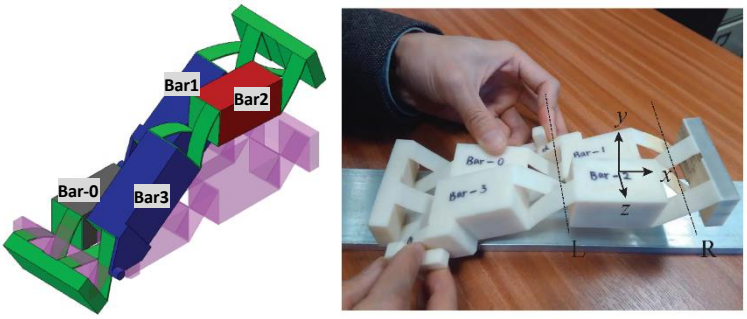

(d) Operation mode IV: Pure translations in the XY-plane along the X and Y axes

Figure 5: Operation modes of the compliant four-bar mechanism

2.2 Kinematic models

The kinematics of the compliant four-bar mechanism is discussed as follows, under the assumption of small angles (i.e., close to the constraint singularity). According to the definition of the location and orientation of the Bar-2 (link BC) with respect to the fixed frame, we can have the primary displacement of the Bar-2 as:

1) Displacement of the centre of Bar-2 along the Y-axis:

$$b-0=l(\sin\alpha+\sin\beta)/2 \approx l(\alpha+\beta)/2 \text{ if small input angles} \quad (2)$$

2) Rotation of Bar-2 about the Z-axis:

$$\phi-0=\alpha-\beta \quad (3)$$

Using the assumption of small angles, the displacement of the centre of Bar-2 along the X-axis is normally in the second order of magnitude of the rotational angles, which is trivial and can be neglected in this paper. Note that this trivial displacement is also affected by the centre drift of the compliant rotational joints [24].

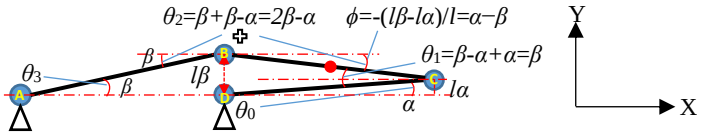

Figure 6: The generic kinematic configuration (close to constraint singularity) of the four-bar linkage

The rotational displacement of each compliant rotational joint is expressed below in terms of the two input rotational angles, with the help of the generic kinematic configuration (Fig. 6):

RJ-0:

$$\theta_0=\alpha \quad (4)$$

RJ-1:

$$\theta_1=\beta \quad (5)$$

RJ-2:

$$\theta_2=2\beta-\alpha \quad (6)$$

RJ-3:

$$\theta_3=\beta \quad (7)$$

3. Design of a multi-mode compliant gripper

3.1 Compliant gripper with multiple modes

In this section, a multi-mode compliant gripper using the compliant four-bar mechanism presented in Fig. 4 as a gripper jaw mechanism is proposed (shown in Fig. 7). Instead of the cross-spring joints in the compliant four-bar mechanism, the commonly-used rectangular short beams as the rotational joints (with rotation axis approximately in the centre) are adopted for the final gripper designed in this paper, as shown in Fig. 7(a). The reason for using the rectangular short beams is mainly twofold. Firstly, comparing with the cross-spring joints, the rectangular joints are compact, simple enough, and easy to fabricate. Secondly, the rectangular joints have larger motion range than that of the circular notch joints (as used in Appendix A). In addition, using the rectangular short-beams allow not to work as pure rotational joints as discussed in Section 2.1.

In order the make the whole mechanism more compact, the compliant gripper is a two-layer structure with two linear actuators to control the two rotational displacements (α and β) in each jaw. The top layer actuator is for determining β, and the bottom layer is for determining α.

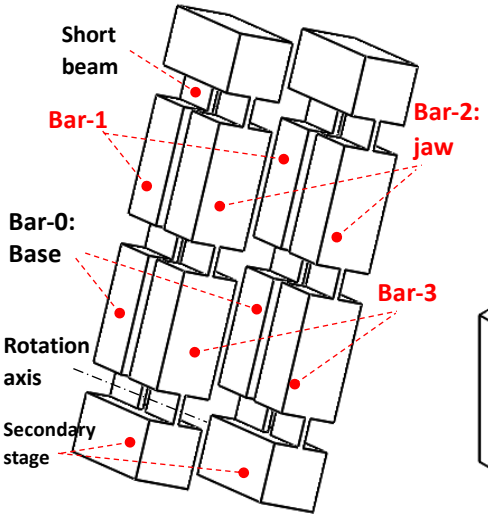

(a) Two gripper jaws in two layers, obtained using the constraint singularity in Fig. 4

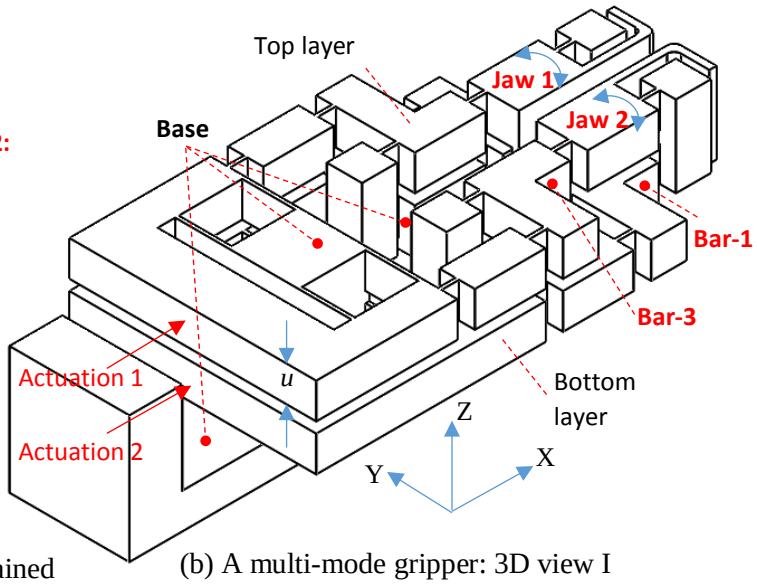

(b) A multi-mode gripper: 3D view I

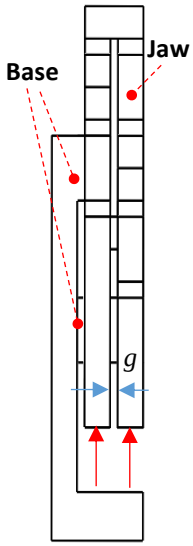

(c) A multi-mode gripper: side view

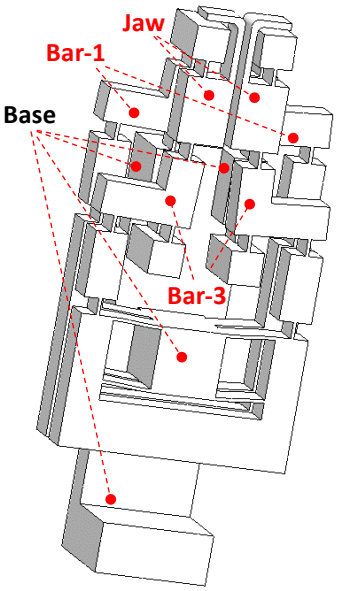

(d) A multi-mode gripper: 3D view II (in deformation)

Figure 7: The synthesized multi-mode compliant gripper

The design of the compliant gripper is further explained in Fig. 8, with all dominant geometrical parameters labelled except the identical out-of-plane thickness (u) of each layer, and the gap (g) between the two layers. As can be seen in Figs. 8(a) and 8(b), a pair of compliant slider-crank mechanism are added in each layer (sharing a revolute joint with the compliant four-bar mechanism), to convert one linear actuation to two simultaneous rotational actuations in two jaws. In both layers, compliant slider-crank mechanisms are identical. All short beams are also identical in the gripper. Each of the L-shaped bars acts as a component of the slider-crank mechanism and also as Bar-1 or -3 as shown in both Figs. 7 and 8. The kinematic schematic of the half gripper is also illustrated in Fig. 8(c) to explain the design principle.

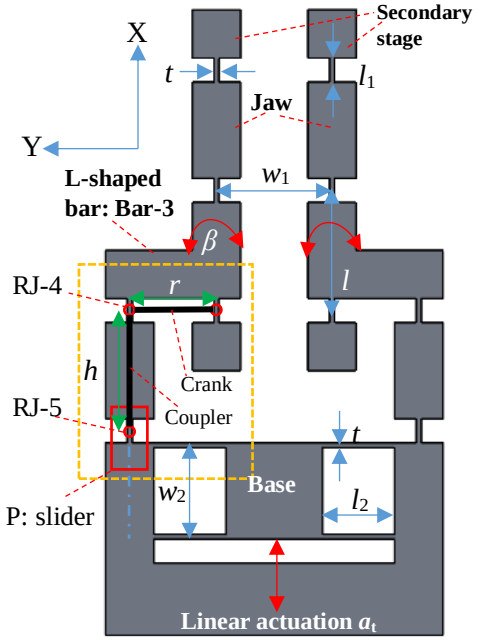

(a) Top layer with two slider-crank mechanisms (indicated by dashed square)

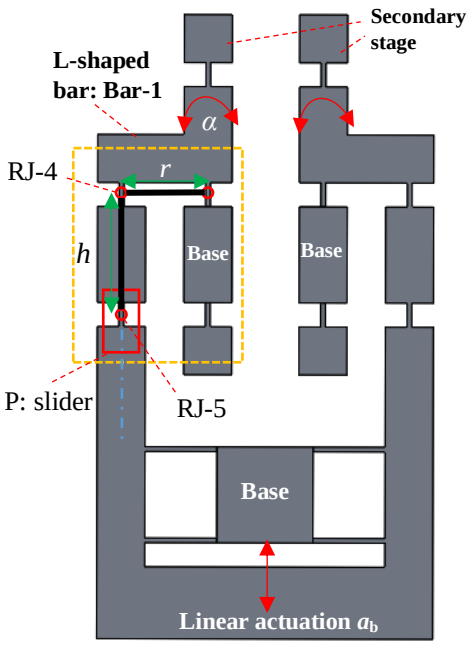

(b) Bottom layer with two slider-crank mechanisms (indicated by dashed square)

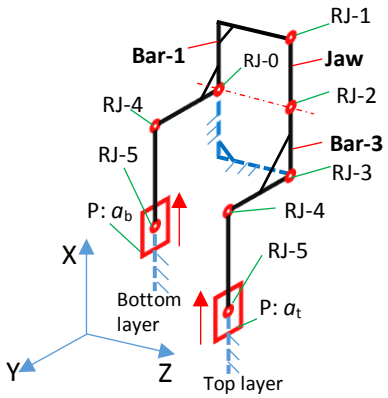

(c) Kinematic schematic of half gripper in the initial configuration

Figure 8: Design details of the multi-mode compliant gripper

3.2 Kinetostatic modelling

Under the assumption of small rotations, the relationship between the linear actuation and the rotational actuation in the slider-crank mechanism (the left jaw is taken for studying) can be modelled below:

$$-a_b = r\alpha \text{ or } \alpha = -a_b/r \tag{8}$$

$$-a_t = r\beta \text{ or } \beta = -a_t/r \tag{9}$$

where a_t and a_b represent the input displacements of the top and bottom actuators along the X-axis, respectively. A minus sign means that the positive linear actuation causes a negative rotational actuation (based on the coordinate system illustrated in Fig. 8). Here, r is the lever arm as shown in Fig. 8.

The rotational displacement of RJ-4 in the added slider-crank mechanism can be approximately obtained as follows. The rotational displacement of RJ-5 in each layer can be ignored due to the specific configuration of the added slider-crank mechanism as shown in Fig. 8, where the crank parallel to the Y-axis is perpendicular to the coupler so that the coupler is approximately straight over motion under the condition of small rotations.

RJ-4 in the top layer:

$$\theta_{4t}=\beta \tag{10}$$

RJ-4 in the bottom layer:

$$\theta_{4b}=\alpha \tag{11}$$

Combining Eqs. (2)-(9), the input-output kinematic equations of the compliant gripper can be obtained:

$$b=-\frac{l}{2r}(a_t+a_b) \tag{12}$$

$$\phi=\frac{a_t-a_b}{r} \tag{13}$$

As indicated in Eqs. (12) and (13), the amplification ratio is a function of design parameter r denoted in Fig. 8. Using the above kinematic equations, the kinetostatic models of the compliant gripper can be derived from the principle of virtual work [3], with a_t and a_b being the generalised coordinates.

$$F_t\mathrm{d}a_t+F_b\mathrm{d}a_b=\frac{\partial U}{\partial a_t}\mathrm{d}a_t+\frac{\partial U}{\partial a_b}\mathrm{d}a_b \tag{14}$$

where F_t and F_b represent the actuation forces of the top and bottom linear actuators along the X-axis, corresponding to a_t and a_b, respectively. U is the total elastic potential energy of the compliant gripper, which is calculated as below:

$$\begin{aligned}\frac{U}{2}&=\frac{1}{2}k_0\theta_0^2+\frac{1}{2}k_1\theta_1^2+\frac{1}{2}k_2\theta_2^2+\frac{1}{2}k_3\theta_3^2+\frac{1}{2}k_4\theta_{4t}^2+\frac{1}{2}k_4\theta_{4b}^2+\frac{1}{2}k_pa_t^2+\frac{1}{2}k_pa_b^2\\&=\frac{1}{2}k_0(\frac{a_b}{r})^2+\frac{1}{2}k_1(\frac{a_t}{r})^2+\frac{1}{2}k_2(\frac{a_b}{r}-2\frac{a_t}{r})^2+\frac{1}{2}k_3(\frac{a_t}{r})^2+\frac{1}{2}k_4(\frac{a_t}{r})^2+\frac{1}{2}k_4(\frac{a_b}{r})^2\\&+\frac{1}{2}k_pa_t^2+\frac{1}{2}k_pa_b^2\end{aligned} \tag{15}$$

where k_0, k_1, k_2, k_3 correspond to the rotational stiffnesses of RJ-0, RJ-1, RJ-2, RJ-3 in the compliant four-bar mechanism, respectively. k_4 is the rotational stiffness of the RJ-4 in each layer. k_p is the translational stiffness of the prismatic joint in each layer.

Note that the reaction forces from gripping objects [17] can be included in Eq. (14), which, however, is not considered in this paper.

Combining the results of Eqs. (14) and (15) with the substitution of Eqs. (4)-(11), we have

$$\begin{aligned}F_t/2&=\frac{\partial U/2}{\partial a_t}=k_1(\frac{a_t}{r})\frac{1}{r}+k_2(\frac{a_b}{r}-2\frac{a_t}{r})(-\frac{2}{r})+k_3(\frac{a_t}{r})\frac{1}{r}+k_4(\frac{a_t}{r})\frac{1}{r}+k_pa_t\\\Rightarrow F_t&=a_t(\frac{2k_1}{r^2}+\frac{8k_2}{r^2}+\frac{2k_3}{r^2}+\frac{2k_4}{r^2}+2k_p)+a_b(\frac{-4k_2}{r^2})\end{aligned} \tag{16}$$

$$\begin{aligned}F_b/2&=\frac{\partial U/2}{\partial a_b}=k_0(\frac{a_b}{r})\frac{1}{r}+k_2(\frac{a_b}{r}-2\frac{a_t}{r})\frac{1}{r}+k_4(\frac{a_b}{r})\frac{1}{r}+k_pa_b\\\Rightarrow F_b&=a_b(\frac{2k_0}{r^2}+\frac{2k_2}{r^2}+\frac{2k_4}{r^2}+2k_p)+a_t(\frac{-4k_2}{r^2})\end{aligned} \tag{17}$$

Equations (16) and (17) can determine the required forces for given input displacements, which can be rearranged in a matrix form:

$$\begin{bmatrix}F_t\\F_b\end{bmatrix}=\begin{bmatrix}k_{11}&k_{12}\\k_{21}&k_{22}\end{bmatrix}\begin{bmatrix}a_t\\a_b\end{bmatrix} \tag{18}$$

where the stiffness coefficients of the system associated with the input forces and input displacements are

$$k_{11}=\frac{2k_1}{r^2}+\frac{8k_2}{r^2}+\frac{2k_3}{r^2}+\frac{2k_4}{r^2}+2k_{\mathrm{p}};$$

$$k_{12}=k_{21}=\frac{-4k_2}{r^2};$$

$$k_{22}=\frac{2k_0}{r^2}+\frac{2k_2}{r^2}+\frac{2k_4}{r^2}+2k_{\mathrm{p}}.$$

Therefore, the input displacements can be represented with regard to the input forces as:

$$\begin{bmatrix} a_{\mathrm{t}} \\ a_{\mathrm{b}} \end{bmatrix}=\begin{bmatrix} c_{11} & c_{12} \\ c_{21} & c_{22} \end{bmatrix}\begin{bmatrix} F_{\mathrm{t}} \\ F_{\mathrm{b}} \end{bmatrix}=\begin{bmatrix} k_{11} & k_{12} \\ k_{21} & k_{22} \end{bmatrix}^{-1}\begin{bmatrix} F_{\mathrm{t}} \\ F_{\mathrm{b}} \end{bmatrix} \tag{19}$$

We can further obtain the following stiffness equations for all compliant joints used in this paper [25], which can be substituted into Eqs. (18) and (19) to solve the load-displacement equations.

$$\begin{aligned} k_0=k_2=k_4&=\frac{EI}{l_1}=\frac{Eut^3}{12l_1} \\ k_1=k_3=k_0/2&=\frac{EI}{2l_1}=\frac{Eut^3}{24l_1} \\ k_{\mathrm{p}}&=\frac{24EI}{l_2^3}=\frac{2Eut^3}{l_2^3} \end{aligned} \tag{20}$$

where E is the Young's modulus of the material and I is the second moment of inertia of the cross-section areas.

With the help of Eqs. (12), (13) and (19), we can have the required output displacements for given input displacements/forces:

$$\begin{bmatrix} b \\ \phi \end{bmatrix}=\begin{bmatrix} -\frac{l}{2r} & -\frac{l}{2r} \\ \frac{1}{r} & -\frac{1}{r} \end{bmatrix}\begin{bmatrix} a_{\mathrm{t}} \\ a_{\mathrm{b}} \end{bmatrix}=\begin{bmatrix} -\frac{l}{2r} & -\frac{l}{2r} \\ \frac{1}{r} & -\frac{1}{r} \end{bmatrix}\begin{bmatrix} k_{11} & k_{12} \\ k_{21} & k_{22} \end{bmatrix}^{-1}\begin{bmatrix} F_{\mathrm{t}} \\ F_{\mathrm{b}} \end{bmatrix} \tag{21}$$

Note that in the above kinetostatic modelling, a linear assumption is made. However, in order to capture accurate load-dependent kinetostatic characteristics for larger range of motion, nonlinear analytical models should be used [26].

4. Case study

In this section, a case study with assigned parameters as shown in Table 1 is presented to verify the analytical models in Section 3.2. The overall nominal dimension of the compliant gripper is 130 mm × 70 mm. The Young's modulus of compliant gripper is given by E=2.4G Pa, which corresponds to the material of Polycarbonate with Yield Strength of σ_s > 60 MPa, and Poisson Ratio of v= 0.38.

Table 1: Geometrical parameters

l	t	r	h	l_1	l_2	w_1	w_2	u	g
25 mm	1 mm	18 mm	25 mm	5 mm	15 mm	24 mm	19 mm	10 mm	3 mm

Finite element analysis (FEA) simulation was carried out to show the four operation modes of the compliant gripper, in comparison to the 3D printed prototype (Fig. 9). Here, Solidworks 2017, with a meshing size of 1.0 mm and other settings, in default is used for FEA. Figure 10 illustrates the comprehensive kinetostatic analysis results of the proposed compliant gripper including the comparison between the analytical modelling and FEA. It can be observed that linear relations of all figures have been revealed where lines in either model are parallel

each other. The FEA results have the same changing trends as the analytical models, but deviate from the analytical models in certain degrees. The discrepancy between the two theoretical models may be due to the assumptions used in the analytical modelling such as neglecting centre drift of rotational joints. It should be pointed out that although stress analysis is not the interest of this paper, the maximal stress (29 MPa) was checked in FEA, which is much less than the yield strength of the material during all simulations for the case study.

In Fig. 10(a), with the increase of a_b, the difference between the two models (analytical and FEA) goes up if a_t=0, while the difference between the two models decreases if a_t=0.50 mm and 1.0 mm. This is because of different line slops of two models. Generally speaking, the larger a_t, the larger the deviation of two models, where the maximal difference in Fig. 10(a) is about 20%. In Fig. 10(b), the line slops of two models are almost same, meaning that the increase of increase of a_b has no influence of the discrepancy of two models for any value of a_t. Also, the larger a_t, the larger the deviation of two theoretical models. Figure 10(c) reveals the same conclusion as that of Fig. 10(b). Figure 10(d) shows the similar finding to that of Fig. 10(a), except the larger a_t, the smaller the deviation of two models. It is clearly shown that in Figs. 10(b), 10(c) and 10(d) the general discrepancy of the two models is much lower than that in Fig. 10(a).

A real prototype made of polycarbonate was fabricated using CNC milling machining, which is shown in Fig.11(a). Each layer of the compliant gripper (Fig. 7) was made at first and then two layers were assembled together. The gripper prototype was tested in a customised-built testing rig as shown in Fig. 11(b). The single-axis force loading for both the top layer actuation and bottom layer actuation was implemented. The micrometer loads displacement on the force sensor that is directly contacted with the top layer input or bottom layer input. The force sensor reads the force exerted on one input of the gripper, and the two displacement sensors indicate the displacements of two inputs. Testing results are illustrated in Fig. 12, which are compared with analytical models and FEA results. It is shown that the analytical displacement result is slightly larger than the experimental model, but is slightly lower than the FEA result. The difference among three models is also reasonable, given that FEA always take all parts as elastic bodies (i.e., less rigid system) and testing is imposed on a prototype with fabricated fillets (i.e., more rigid system).

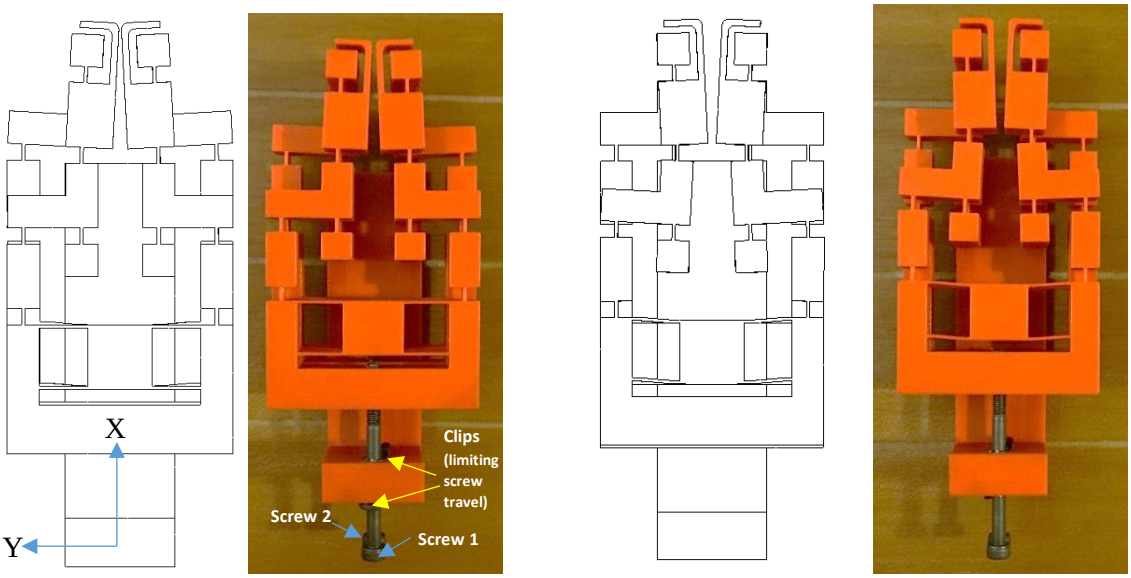

(a) a_b=1 mm, a_t= 0

(b) a_t =1 mm, a_b= 0

(c) a_t=1 mm, a_b =0.5 mm

(d) a_b=a_t=1 mm

Figure 9: Gripper operation modes under input displacement control

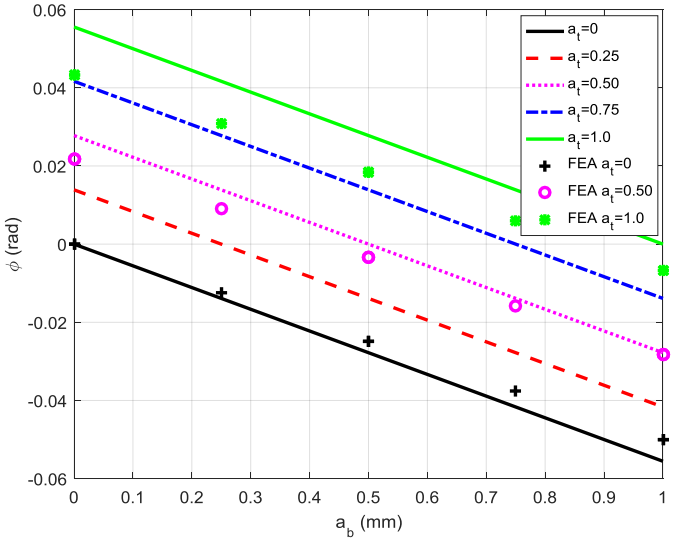

(a) Output rotational angle about the Z-axis

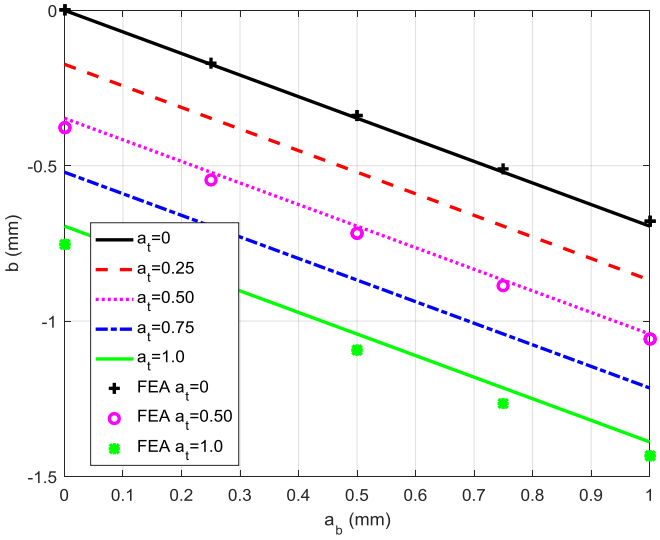

(b) Output displacement along the Y-axis

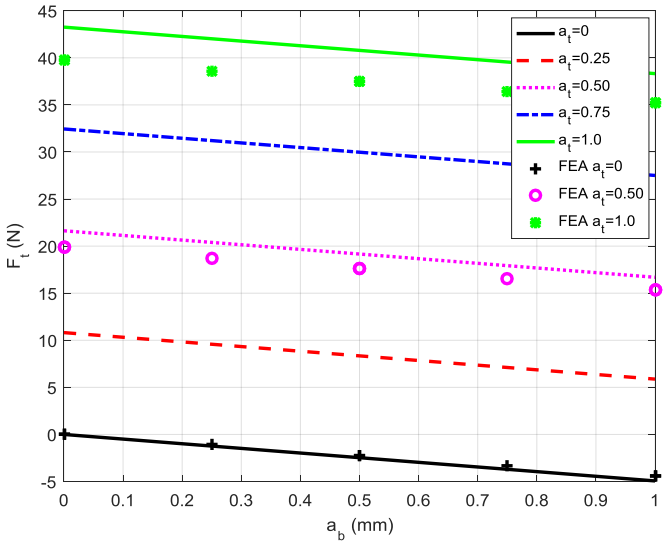

(c) Input force exerted onto the top layer

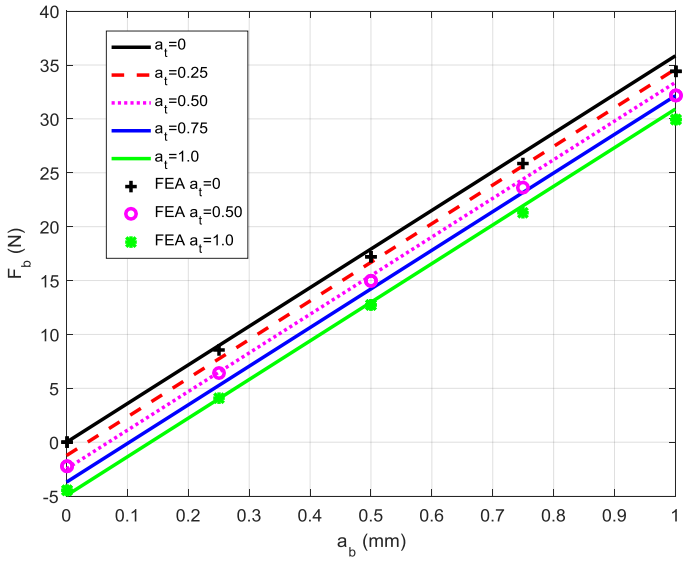

(d) Input force exerted onto the bottom layer

Figure 10: Comprehensive analysis under displacement control (input displacement non-negative)

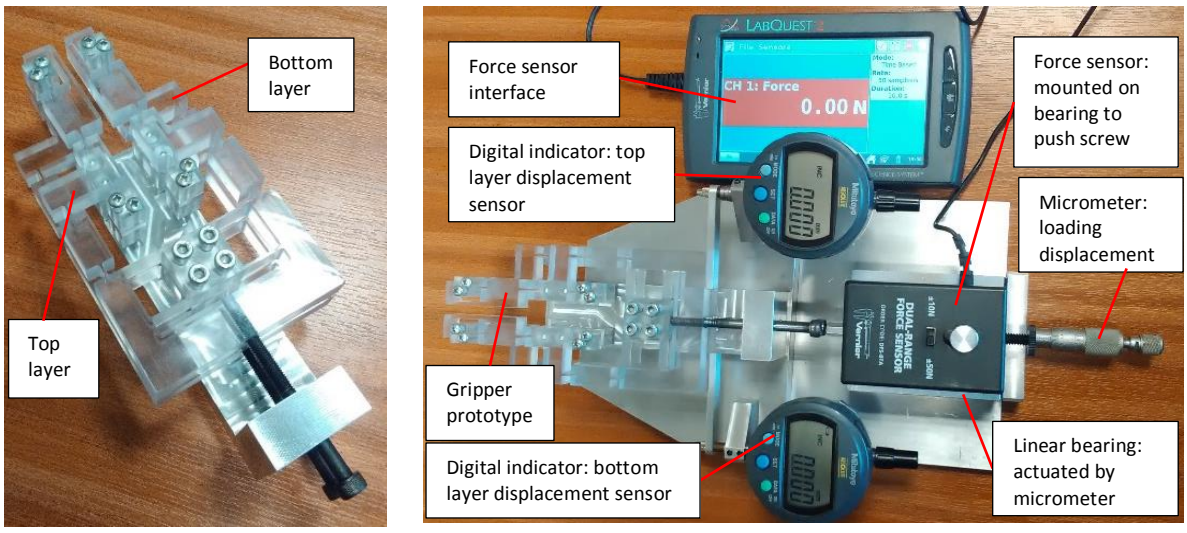

(a) Assembled prototype

(b) Testing rig

Figure 11. A fabricated polycarbonate prototype and its testing

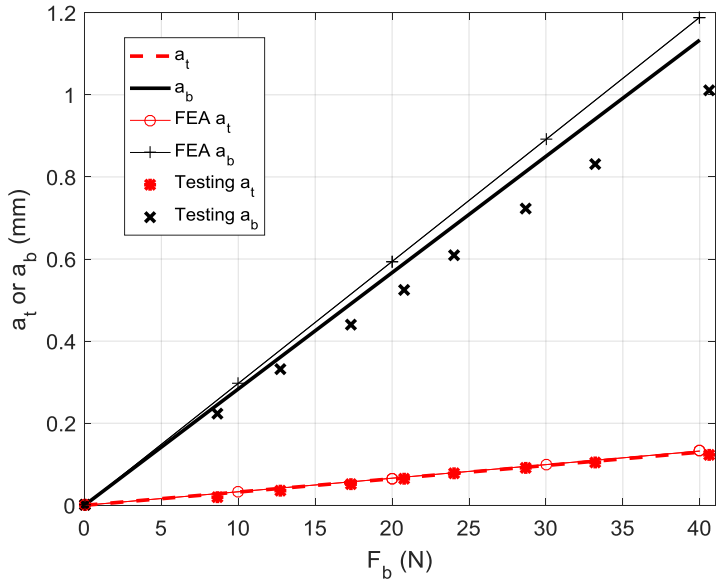

(a) Case for F_t=0

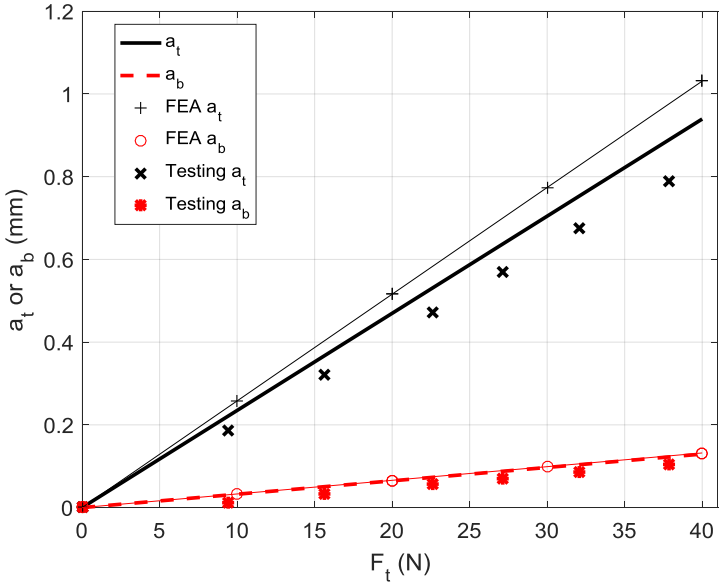

(b) Case for F_b=0

Figure 12. Input-force and input-displacement comparisons under single-axis force loading

5. Conclusions

In this paper, we present the first piece of work that employs a constraint singularity of a planar equilateral four-bar linkage to design a reconfigurable compliant gripper with multiple operation modes. The analytical kinetostatic mode of the multi-mode compliant gripper has been derived, which is verified in the case study. It shows that the FEA results comply with the analytical models with acceptable discrepancy. The proposed gripper is expected to be applied in extensive applications such as grasping a variety of shapes or adapting to specific requirements.

The design introduced in this paper uses a two-layer configuration for desirable compactness, which adversely results in non-desired small out-of-plane rotations. However, the out-of-plane rotations can be reduced by optimising currently-used compliant joints or employing different compliant joints with higher out-of-plane

stiffness. Note that the compliant gripper can be designed in a single layer for monolithic fabrication and elimination of out-of-plane motion, at the cost of a larger footprint. This can be done by using the remote rotation centre, as shown in Appendix A. A single layer gripper can be more easily designed at micro-scale on a silicon layer for MEMS devices.

Despite the work mentioned above, there are other aspects to be considered in the future, including but not limited to the following: (*i*) An analytical nonlinear model for a more accurate large-range kinetostatic modelling of the compliant gripper; (*ii*) Design optimisation the compliant gripper based on a specific application; (*iii*) Output testing with comparison to the analytical model for a specific application; and (*iv*) Developing a control system to robotise the compliant gripper.

Acknowledgment
The author would like to thank Mr. Tim Power and Mr. Mike O'Shea from University College Cork for the excellent prototype fabrication work as well as their kind assistance in the experimental testing. The work in this paper was funded by IRC Ulysses 2015/2016 grant.

References

[1] Verotti, M., Dochshanov, A., and Belfiore, N.P., 2017, A Comprehensive Survey on Microgrippers Design: Mechanical Structure, ASME Journal of Mechanical Design, 139(6):060801-060801-26. doi:10.1115/1.4036351.
[2] Nordin, M. and Gutman, P.O., 2002, Controlling mechanical systems with backlash-a survey, Automatica, 38 (10):1633-1649.
[3] Howell, L. L., 2001, Compliant Mechanisms, Wiley, New York.
[4] Zhu, B., Zhang, X., and Wang, N., 2013, Topology optimization of hinge-free compliant mechanisms with multiple outputs using level set method, Structural and Multidisciplinary Optimization, 47(5): 659-672.
[5] Hao, G., and Li, H., 2015, Conceptual designs of multi-degree of freedom compliant parallel manipulators composed of wire-beam based compliant mechanisms. Proceedings of the Institution of Mechanical Engineers, Part C: Journal of Mechanical Engineering Science, 229(3), pp.538-555.
[6] Wang, M. Y., Chen, S., Wang. X., et al, 2005, Design of Multimaterial Compliant Mechanisms Using Level-Set Methods, ASME Journal of Mechanical Design, 127(9): 941-956.
[7] Amine, S., Mokhiamar, O., and Caro, S., 2017. "Classification of 3T1R parallel manipulators based on their wrench graph". ASME Journal of Mechanisms and Robotics, 9(1).
[8] Maraje, S., Nurahmi, L., and Caro, S., 2016. "Operation modes comparison of a reconfigurable 3-PRS parallel manipulator based on kinematic performance." In Proceedings of the ASME 2016 International Design Engineering Technical Conferences and Computers and Information in Engineering Conference. pp. 21–24.
[9] Nurahmi, L., and Caro, S., 2015. "Dimensionally homogeneous extended jacobian and condition number." In The 2nd International Conference on Mechanical Engineering (ICOME 2015). pp. 3–5.
[10] Rubbert, L., Caro, S., Gangloff, J., and Renaud, P., 2014. "Using singularities of parallel manipulators for enhancing the rigid-body replacement design method of compliant mechanisms". ASME Journal of Mechanical Design, 136, pp. 051010–1–051010–9.
[11] Rubbert, L., Renaud, P., Caro, S., and Gangloff, J., 2014. "Design of a compensation mechanism for an active cardiac stabilizer based on an assembly of planar compliant mechanisms". Mechanics & Industry, 15(2), pp. 147–151.
[12] Zlatanov, D., Bonev, I. A., and Gosselin, C. M., 2002. Constraint Singularities as C-Space Singularities. Springer Netherlands, Dordrecht, pp. 183–192.
[13] Husty, M. L., Pfurner, M., Schröcker, H.-P., and Brunnthaler, K., 2007. "Algebraic methods in mechanism analysis and synthesis". Robotica, 25(6), Nov., pp. 661–675.
[14] Nurahmi, L., Caro, S., Wenger, P., Schadlbauer, J., and Husty, M., 2016. "Reconfiguration analysis of a 4-RUU parallel manipulator". Mechanism and Machine Theory, 96, Part 2, pp. 269 – 289.
[15] He, X., Kong, X., Hao, G., and Ritchie, J., 2016. Design and Analysis of a New 7R Single-Loop Mechanism with 4R, 6R and 7R Operation Modes. Springer International Publishing, Cham, pp. 27–37.

[16] Beroz, J.D., Awtar, S., Bedewy, M., Sameh, T., and Hart, A.J., 2011, Compliant microgripper with parallel straight-line jaw trajectory for nanostructure manipulation, Proceedings of 26th American Society of Precision Engineering Annual Meeting, Denver, USA.
[17] Hao, G., and Hand, R.B., 2016, Design and static testing of a compact distributed-compliance gripper based on flexure motion, Archives of Civil and Mechanical Engineering, 16(4):708-716.
[18] Hao, G., 2015, "Mobility and Structure Re-configurability of Compliant Mechanisms", Mechanism and Machine Science, Vol. 36, Xilun Ding et al. (Eds): Advances in Reconfigurable Mechanisms and Robots II, 978-3-319-23326-0, 334477_1_En, Berlin: Springer (chapter 5)
[19] Hao, G., Li, H., and Kavanagh, R. C., 2016. "Position space-based compliant mechanism reconfiguration approach and its application in the reduction of parasitic motion." ASME. J. Mech. Des., 138(9), pp. 092301–092301–13.
[20] Birglen, L., Polyvalor and Limited Partnership, 2015. Self-adaptive mechanical finger and method. U.S. Patent 9,126,342.
[21] Laliberté, T., Birglen, L. and Gosselin, C., 2002. Underactuation in robotic grasping hands. Machine Intelligence & Robotic Control, 4(3), pp.1-11
[22] Nayak, A., Li, H., Hao, G., Caro, S., 2017, "A Reconfigurable Compliant Four-Bar Mechanism with Multiple Operation Modes", ASME 2017 International Design Engineering Technical Conferences & Computers and Information in Engineering Conference, August 6-9, 2017 in Cleveland, Ohio (DETC2017-67441)
[23] Henein, S., Rubbert, L., Cosandier, F., Richard, M., 2017, "The art of flexure mechanism design", EPFL Press, Lausanne。
[24] Zhao, H., Bi, S., and Yu, J., 2012. "A novel compliant linear-motion mechanism based on parasitic motion compensation". Mechanism and Machine Theory, 50, pp. 15 –28.
[25] Hao, G. and He, X., 2017. Designing a monolithic tip-tilt-piston flexure manipulator. Archives of Civil and Mechanical Engineering, 17(4), pp.871-879.
[26] Ma, F. and Chen, G., 2016. Modeling large planar deflections of flexible beams in compliant mechanisms using chained beam-constraint-Model. Journal of Mechanisms and Robotics, 8(2), p.021018.

Appendix A: A monolithic design of the compliant gripper

Rather than using a two-layer mechanism as shown in Figs. 6 and 7, a single layer mechanism is presented in Fig. A.1, which is good for monolithic fabrication and can eliminate out-of-plane motion. In order to reach the constraint singularity, i.e. allowing the overlapping of two revolute joints, the design uses isosceles trapezoidal flexure joints with remote center of rotation. However, this one layer mechanism has a quite large footprint, and requires more extra space for incorporating the two actuators. Moreover, due to the use of circular notch joints, operation modes II and III in this gripper may not produce large-range motion. The modelling and analysis of the present monolithic design in this appendix is left for future study.

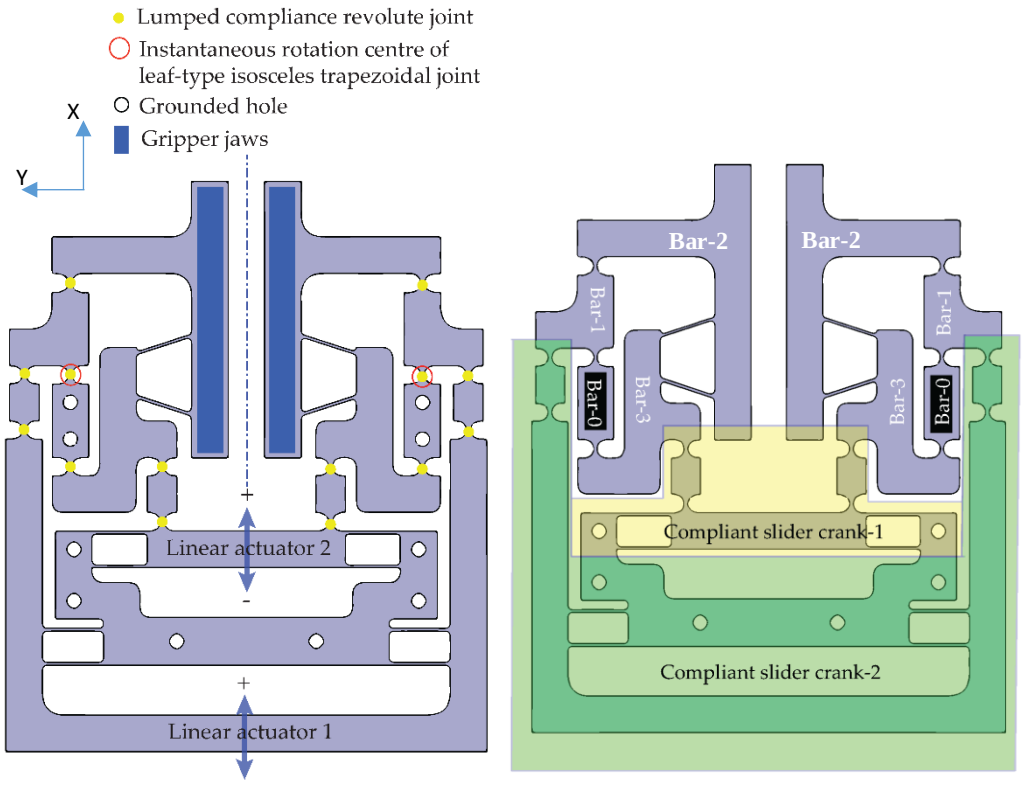

(a) Monolithic design of the reconfigurable compliant gripper

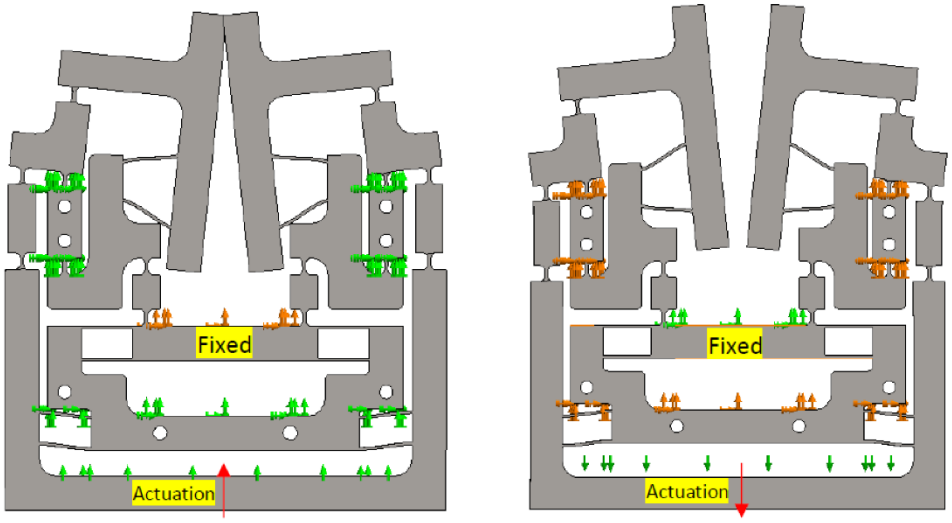

(b) Actuating the linear actuator 1 only in bi-directions

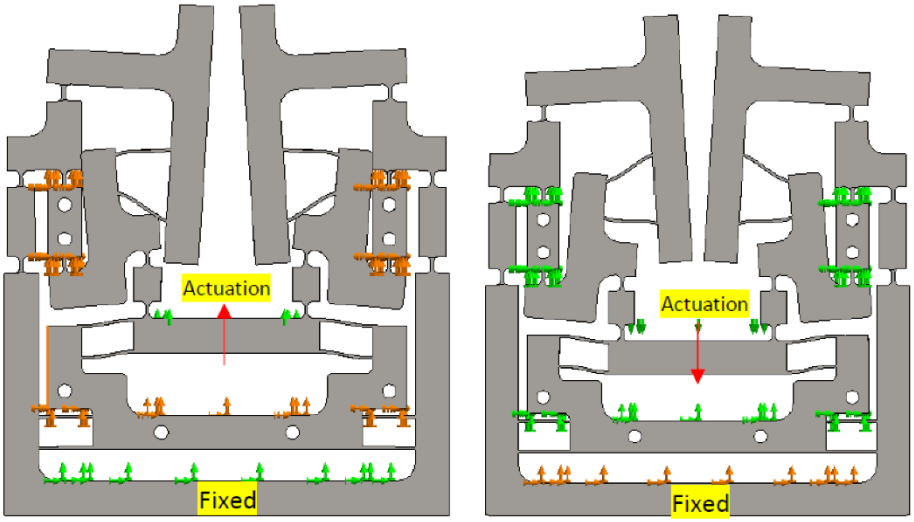

(c) Actuating the linear actuator 2 only in bi-directions

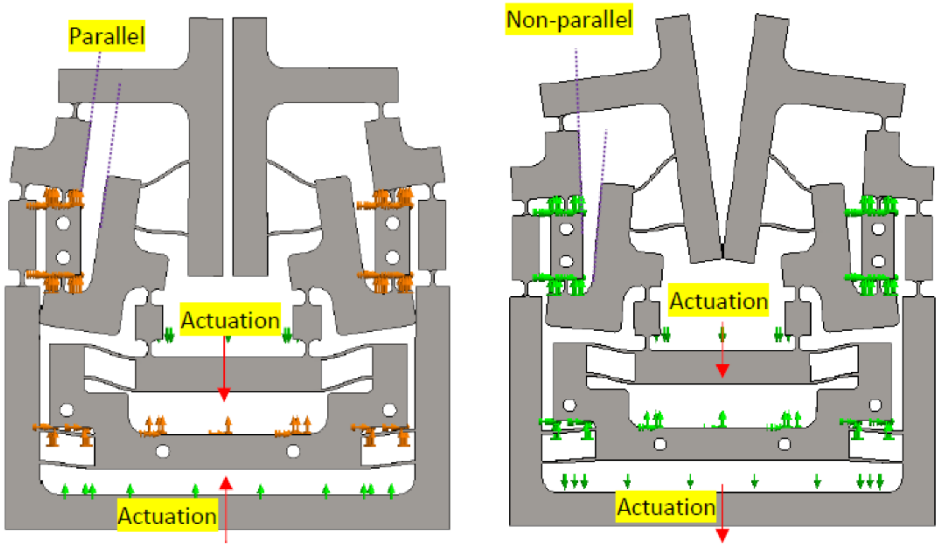

(d) Actuating the two linear actuators simultaneously: parallel grasping mode (left); general angular grasping mode (right)

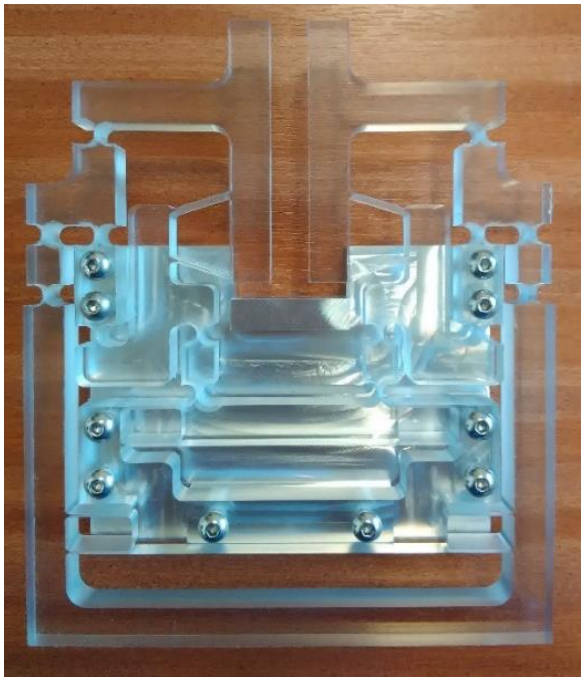

(e) Fabricated prototype

Figure A.1: Monolithic design of the reconfigurable gripper